HHS Public Access

Author manuscript

Microvasc Res. Author manuscript; available in PMC 2016 September 01.

Published in final edited form as:

Microvasc Res. 2015 September ; 101: 86–95. doi:10.1016/j.mvr.2015.07.001.

Evaluation of the effect of elevated intraocular pressure and reduced ocular perfusion pressure on retinal capillary bed filling and total retinal blood flow in rats by OMAG/OCT

Zhongwei Zhi[a], **William Cepurna**[b], **Elaine Johnson**[b], **Hari Jayaram**[b], **John Morrison**[b], and **Ruikang K. Wang**[a,c,*]

[a]Department of Bioengineering, University of Washington, Seattle, WA 98195, USA

[b]Casey Eye Institute, Oregon Health & Science University, Portland, OR 97239, USA

[c]Department of Ophthalmology, University of Washington, Seattle, WA 98195, USA

Abstract

Purpose—To determine if retinal capillary filling is preserved in the face of acutely elevated intraocular pressure (IOP) in anesthetized rats, despite a reduction in total retinal blood flow (RBF), using optical microangiography/optical coherence tomography (OMAG/OCT).

Methods—OMAG provided the capability of depth-resolved imaging of the retinal microvasculature down to the capillary level. Doppler OCT was applied to measure the total RBF using an *enface* integration approach. The microvascular pattern, capillary density, and total RBF were monitored in vivo as the IOP was increased from 10 to 100 mm Hg in 10 mm Hg intervals and returned back to 10 mm Hg.

Results—In animals with mean arterial pressure (MAP) of 102 ± 4 mm Hg (n = 10), when IOP was increased from 0 to 100 mm Hg, the capillary density remained at or above 80% of baseline for the IOP up to 60 mm Hg [or ocular perfusion pressure (OPP) at 40 mm Hg]. This was then decreased, achieving 60% of baseline at IOP 70 mm Hg and OPP of 30 mm Hg. Total RBF was unaffected by moderate increases in IOP up to 30 mm Hg, beyond which total RBF decreased linearly, reaching 50% of baseline at IOP 60 mm Hg and OPP 40 mm Hg. Both capillary density and total RBF were totally extinguished at 100 mm Hg, but fully recovered when IOP returned to baseline. By comparison, a separate group of animals with lower MAP (mean = 75 ± 6 mm Hg, n = 7) demonstrated comparable decreases in both capillary filling and total RBF at IOPs that were 20 mm Hg lower than in the initial group. Both were totally extinguished at 80 mm Hg, but fully recovered when IOP returned to baseline. Relationships of both parameters to OPP were unchanged.

Conclusion—Retinal capillary filling and total RBF responses to IOP elevation can be monitored non-invasively by OMAG/OCT and both are influenced by OPP. Retinal capillary filling was relatively preserved down to a perfusion pressure of 40 mm Hg, despite a linear reduction in total RBF.

*Corresponding author at: University of Washington, Department of Bioengineering, Seattle, Washington 98195, USA. wangrk@uw.edu (R.K. Wang).

Keywords

Retinal blood flow; Intra-ocular pressure; Optical coherence tomography; Medical and biological imaging; Optical microangiography

Introduction

Glaucoma, a leading cause of blindness, involves irreversible optic nerve damage (Quigley and Broman, 2006). Although many glaucoma risk factors have been identified, elevated intraocular pressure (IOP) is the best defined, and controlling IOP is the mainstay of contemporary glaucoma therapy (Sommer, 1989). To date, many studies have been conducted to evaluate the effect of increased IOP upon the retina and optic nerve head (ONH) (Strouthidis et al., 2011; Fortune et al., 2004; Vidal et al., 2006; Johnson et al., 2011; Kim et al., 1998; Yancey and Linsenmeier, 1989; Ruusuvaa and Palkama, 1974; Alm and Bill, 1972; Bui et al., 2005). Unfortunately, the underlying mechanisms of how IOP leads to glaucomatous optic nerve damage are still not fully understood (Morrison et al., 2005). It remains unclear whether the elevated IOP damages the ONH and retina directly (Zeimer, 1989; Roberts et al., 2010), or whether the accompanying ischemic insult due to reduced ocular perfusion pressure exerts an additional effect (Pillunat et al., 1996, 1997; Liang et al., 2009a). Animal models are necessary to study these mechanisms in more detail. Utilizing chronic IOP elevation in rats, experimental glaucoma has provided a useful tool for understanding the complex mechanisms that lead to the development and progression of glaucomatous optic nerve damage. (Morrison et al., 1997, 2005, 2008, 2011; Fortune et al., 2011; Pang and Clark, 2007).

Several laboratories have also used short-term elevations in IOP, from 30 min to several hours, as a unique approach to determine ONH and retinal responses to IOP (Abbott et al., 2014; Balaratnasingam et al., 2007, 2008; Sun et al., 2013). Others have combined experimental glaucoma with electroretinography (ERG) as a non-invasive test to measure the impact of short term IOP exposures on the ONH and retina, and have used this system to determine the effects of age, dietary restriction and mitochondrial abnormalities on their response (Kong et al., 2011, 2012). However, the exact contribution of ischemia to this response is currently unknown. Detailed assessment has shown that acute IOP elevation has a differential effect on the various components of the ERG, depending on the level of pressure (Bui et al., 2005). More recently, 90 minute variations were shown to not produce permanent ERG changes unless the IOP was higher than 60 mm Hg (Bui et al., 2013). However, analysis of ocular blood flow indicates that retinal blood flow is more sensitive, demonstrating a reduction to well below 50% of baseline at this level of pressure (He et al., 2012; Zhi et al., 2012a). He and colleagues have proposed that retinal function is maintained in the face of this reduced total blood flow by a compensatory increase in oxygen extraction (He et al., 2013). Anatomic support for this hypothesis depends on the ability to image and monitor retinal capillary filling.

Currently there is no technique available for retinal capillary visualization, other than adaptive optics scanning laser ophthalmoscopy (AOSLO) (Roorda et al., 2002; Pinhas et al.,

2014). However, AOSLO requires complex adaptive optical systems and usually requires injection of fluorescent dye to image blood vessels. There are a number of methods used for studying retinal blood flow (RBF). Dye dilution (Ffytche et al., 1974) involves the use of tracing fluorescent dyes flowing in the retinal vessels to determine the flow velocity. However, the dye injection is not comfortable for patients, and this, in itself, may produce unpredictable side effects. Laser Doppler velocimetry (LDV) (Shepherd and Riedel, 1982) is a commonly used technique for flow velocity measurement in the retina; however, it does not provide sufficient spatial resolution. Laser speckle flowgraphy, which is based on the laser speckle phenomenon, has been used in monkeys to evaluate the relationship between systemic blood pressure and optic nerve head blood flow (Liang et al., 2009b), but it is not capable of providing a 3D map of the vasculature. Therefore, there is still a need for noninvasive techniques that can be used to obtain both volumetric visualization of the vasculature and absolute measurements of RBF with high resolution.

Optical coherence tomography (OCT) (Huang et al., 1991; Tomolins and Wang, 2005) is an established tool for measuring the peripapillary retinal nerve fiber layer (NFL) thickness, which is affected by glaucomatous damage (Kanamori et al., 2003; Schuman et al., 1995; Guedes et al., 2003). Current applications of OCT in experimental glaucoma have primarily focused on detecting structural changes in response to elevated IOP (Fortune et al., 2011; Abbott et al., 2014; Srinivasan et al., 2006; Ruggeri et al., 2007; Guo et al., 2010). Optical microangiography (OMAG) (Wang et al., 2007, 2010; An et al., 2010), an adaptation of Fourier domain OCT (FD-OCT), is a novel imaging modality that is capable of generating 3D images of dynamic blood perfusion distribution within microcirculatory tissue beds. This ability to visualize detailed capillary networks and quantify the total retinal blood flow (RBF) in experimental glaucoma would help advance our understanding of the impact of elevated IOP on ocular blood flow. In our previous work (Zhi et al., 2011, 2012a), we evaluated the effect of elevated IOP on the structure and blood flow of the retina, choroid and ONH in rats using OMAG. Due to the limited system resolution, it was difficult to evaluate retinal capillary bed responses to increased IOP. To solve this problem, we have developed an ultra-high resolution OCT system for imaging the rodent retina. By applying ultra-high sensitive OMAG methods (An et al., 2010; Wang et al., 2010), we are now able to provide capillary resolution and depth-resolved retinal vascular perfusion maps in rodents (Zhi et al., 2012b, 2014).

A further limitation of our previous work (Zhi et al., 2011, 2012a) is that the effect of increased IOP upon RBF was only evaluated on selected retinal arteries and veins. We were unable to evaluate the total RBF. In order to quantify total blood flow, it is necessary to know a priori the Doppler angle of each vessel, which is susceptible to errors for the blood flow calculation. In this work, we utilize an *en face* Doppler OCT approach, originally proposed by Srinivasan et al. (2010) to measure the total RBF in rats. In this way, the flow can be calculated by integrating the axial blood flow velocity over the vessel area measured in an *en face* plane without knowing the blood vessel angle. This approach allows us to non-invasively evaluate the effect of acutely elevated IOP on total RBF, as well as retinal capillary filling.

Systemic blood pressure may also play an important role in glaucoma (Liang et al., 2009a; He et al., 2011). In these experiments, we now incorporate the monitoring of mean arterial blood pressure (MAP) throughout the process of IOP elevation. This allowed us to evaluate the effect of ocular perfusion pressure (OPP) (MAP-IOP), instead of IOP alone, on retinal blood flow and capillary filling in two groups of animals, representing distinct levels of MAP.

Materials and experimental methods

System setup and methodology

Fig. 1 shows the schematics of the custom-built high-speed SD-OCT system setup for in vivo imaging of the rat retina under elevated IOP. Briefly, the system was operated at a central wavelength of 840 nm with a spectral bandwidth of 42 nm, providing an axial resolution of approximately 7.2 μm in air. The custom-built spectrometer encloses a high-speed CMOS line scan camera (Basler Sprint spL 4096–140 km), having 10 μm square pixels in two rows and 4096 pixels wide. In order to increase the camera speed, only 896 pixels were utilized and the camera was read at an exposure time of 2.9 μs, which provided an ultra-fast line scan rate of 240 kHz. In the sample arm, we applied an objective lens (75 mm focal length) and ocular lens (Ocular Instrument, Maxlight Standard 90D) combination that enables a large field of view and a lateral resolution (~10 μm, simulated results with Zemax) of the rat retina. The total depth range was measured to be ~2.5 mm in air. The power of the OCT beam at the cornea of the rat eye was ~1.2 mW. The measured signal to noise ratio (SNR) was ~100 dB at the focus spot of the sampling beam, which was ~0.5 mm below the zero delay line. The system had a 6 dB sensitivity roll-off at a depth of ~1.5 mm.

Ten adult brown Norway rats with an average body weight of ~ 300 g were used in this study. The rats were anesthetized with inhalational isoflurane (2.0%) mixed with pure oxygen and positioned in a custom-made holding stage with multi-dimensional adjustability. Under isoflurane anesthesia, the tail artery was cannulated and connected to a pressure transducer to monitor MAP throughout the entire experiment. In order to maintain a relatively moderate and stable MAP, we employed an active pump to evacuate expired isoflurane and CO_2. The body temperature was kept at 37 °C by a homeothermic blanket control unit.

All animal procedures were approved by the Animal Care and Use Committee of the Oregon Health and Science University and the University of Washington. For each animal, the right eye was studied. The IOP was elevated unilaterally by cannulation of the anterior chamber with a 31 gage needle shortened to 5 mm and connected to a reservoir filled with balanced salt solution (BSS Plus, Alcon Laboratories Inc.) and to a calibrated pressure transducer (Fig. 1). Topical anesthetic (0.5% proparacaine hydrochloride, Alcon Laboratories Inc.) was instilled for added corneal anesthesia prior to cannulation. The height of the reservoir was adjusted in order to elevate IOP, as determined by the transducer, in 10 mm Hg increments, from 10 mm Hg (treated as baseline) to 100 mm Hg, which produced complete obstruction of ocular blood flow. IOPs were intermittently monitored indirectly for confirmation during cannulation with a rodent tonometer (Tonolab, iCare, Finland). IOP was then returned to baseline (10 mm Hg) so that reperfusion could be measured.

After cannulation, the eye was carefully placed under the sample arm for OCT imaging. Before OCT imaging, the pupil was dilated with 1% tropicamide and 2.5% phenylephrine to allow the OCT beam access to the posterior segment and normal saline solution was applied to maintain corneal hydration during the experiment.

Data acquisition

At each IOP level, a 3-dimensional data volume with an *en face* area of ~2 × 2 mm^2 that included the ONH and adjacent retina was first captured using the ultrahigh sensitive OMAG step scanning protocol (Wang et al., 2010), in which the raster scanning of the beam spot was performed to capture 512 A-lines within each B-frame (2D cross-sectional image) and 2000 B-frames for each C-scan (3D image). These 2000 B-frames were captured at 400 cross-sections with 5 repeated B-frames captured at each cross-section. Using a frame rate of 360 frames per second (fps), the whole 3D data volume could be captured within 5.5 s. We then captured another 3D dataset covering a region of ~1 × 1 mm^2 around the ONH using the Doppler OCT scanning protocol with dense A-scan (2000 A-lines per B-frame) for phase-resolved Doppler OCT analysis to determine the axial blood flow velocity. In this case, the camera acquisition rate was reduced to 140,000 A-scans per second, resulting in a frame rate of 56 fps. The system has a real time preview function to make sure the ONH was placed near the center of the imaging area. Between each IOP elevation and data acquisition, there was a 2 minute interval to allow stabilization before data acquisition. The whole time period for a series of experiments was about 30 min when IOP was increased from 10 to 100 mm Hg in 10 mm Hg intervals and returned back to 10 mm Hg.

Depth-resolved microvasculature imaging with OMAG and quantification

The 3D OMAG data were post-processed using the ultrahigh sensitive OMAG algorithm (An et al., 2010; Wang et al., 2010; Yousefi et al., 2011). Breifly, at each cross-section, the five phase-compensated complex signals of B-frames were subtracted subsequently and then averaged (four times) to obtain the cross-sectional blood flow image. This was applied to all of the 400 cross-sections to generate concurrent 3D structural and blood flow movies.

The rodent retina consists of three layers of vascular networks (Zhi et al., 2014; Cuthbertson and Mandel, 1986): retinal arteries and veins along with the radial peripapillary capillaries within the NFL and ganglion cell layer (GCL), the intermediate capillary networks within the inner plexiform layer (IPL), and the deep capillary networks within the outer plexiform layer (OPL).To better show this retinal vessel distribution and quantify the microvascular response to elevated IOP, we investigated the microvascular maps in these different layers. To do so, a semi-automated retinal layer segmentation algorithm developed by our research group (Yin et al., 2014) was used to segment individual retinal layers from the OCT cross-sectional structural images using a two double line model. The segmentation was first applied on structural images and then directly transferred to blood flow images.

To better quantify the capillary response to the elevated IOP, the capillary density of the OPL was calculated as the pixel number occupied by capillaries over the total pixel number on the binarized image (Reif et al., 2012). We chose to quantify the OPL but not IPL because the tailing effect from superficial vessels was less pronounced in the OPL capillary

bed. Percentages of capillary vessel density at each IOP level, normalized to the baseline (10 mm Hg), were then calculated and plotted. Using MAP, OPP was calculated at each pressure level and then capillary density, again normalized to baseline, was plotted vs OPP.

Measurement of total retinal blood flow rate by en face Doppler OCT

We utilized an *en face* Doppler OCT approach proposed by Srinivasan et al. (2010) to measure the total RBF. This was calculated by integrating the axial blood flow velocity over the vessel area measured in an *en face* plane without knowing a priori the blood vessel angle. Since the entire retinal blood flow in the rat eye is supplied by the central retinal artery (CRA) and is collected by the central retinal vein (CRV), the total RBF rate could be calculated as either the sum of all major retinal arteries or the sum of all major retinal veins. For this study, we calculated total RBF as the average of arterial and venous blood flow rate using the same approaches we developed for total RBF rate measurement in our mouse study (Zhi et al., 2012b). The effect of acutely elevated IOP on total RBF was evaluated, as well as the changes in total RBF versus OPP.

Results

OMAG/OCT provides unprecedented details of the rat retinal vasculature

This OMAG/OCT system provided high resolution cross-sectional imaging of the rat retina (Fig. 2A), which illustrates all the physiological retinal layers. Three dimensional rendering of the imaged retina (Fig. 2B) was obtained using 3D visualization software. Fig. 2C shows the OCT fundus image, (similar to the image captured by 2D cameras), where limited detail of the retina, e.g., optic nerve head and some large retinal vessels, but not capillary vessels. To better show the details of the retina at different depths, we segmented the retina into different physiological layers. The innermost layer was the nerve fiber layer (Fig. 2D), giving ability to visualize optic nerve fiber bundles.

Microvascular maps in the three different retinal layers as well as the choroid were obtained as shown in Fig. 2 (E–H), from which different vascular patterns are observed. The retinal arteries and veins, along with peripapillary capillaries, exist within the NFL and GCL, where they are arranged alternately and radiate in spoke-like fashion towards the retinal periphery (Fig. 2E). Dense, intermediate capillary networks are well distributed and observed in the IPL, where they supply the inner retina (Fig. 2F). The OPL consists of capillary networks and post-capillary venules (Fig. 2G) that supply nutrients to the outer retina. The choroidal vasculature (Fig. 2H) is mainly made up of large vessels, although smaller blood vessels were also observed around the ONH. Details of the dense capillary network of the choriocapillaris were beyond the resolution of the current system.

OMAG can visualize and quantify the effect of elevated IOP on retinal capillary beds

The mean tail arterial blood pressure, which was treated as MAP, was monitored throughout each experiment. The MAP over all experiments ranged from 95 to 120 mm Hg (mean = 102 ± 4 mm Hg (± SEM, n = 10)), indicating negligible variation in MAP over the entire measurement session.

Figs. 3 and 4 illustrate OMAG microangiograms, showing the response of the NFL/GCL, IPL and OPL of the rat retinal microvasculature around the optic disc to step-wise increases in IOP. Qualitatively, no change was observed in vessel appearance when the IOP was increased from 10 mm Hg to approximately 60–70 mm Hg. Above this level, the density of the capillaries and the diameters of major arteries and veins appeared to decrease, a process that was particularly obvious above 80 mm Hg IOP. For all layers, vessel appearance returned to normal once IOP was returned to 10 mm Hg.

In order to better evaluate the effects of elevated IOP on retinal capillary bed filling, the capillary density of the outer plexiform layer (OPL), where the tailing effect from overlying larger retinal vessels appears the least, was quantified using the OMAG images. OPL capillary density remained at or above 80% of baseline up to IOP 60 mm Hg. (Fig. 5A) Above 60 mm Hg, capillary density decreased, reaching 60% of normal at IOP 70 mm Hg and zero at 100 mm Hg, confirming our qualitative assessment of the microangiography images in Figs. 3 and 4.

OPL capillary density was then analyzed as a function of OPP. A polynomial fitting applied to these data gave a curve (Fig. 5B) mathematically relating OPL capillary density to perfusion pressure ($R^2 = 0.95$), showing less than 20% reduction in capillary density as long as OPP was greater than 40 mm Hg. With OPP lower than 40, capillary density decreased abruptly, reaching 60% of normal at 30 mm Hg perfusion pressure and zero as OPP neared zero.

Based on these results, the capillary bed filling of the rat retina remained above 80% of baseline up to an IOP of 60 mm Hg, or perfusion pressure greater than 40 mm Hg. Capillary density was reduced to less than 60% of baseline when IOP exceeded 70 mm Hg, corresponding to an OPP of less than 30 mm Hg. Capillaries showed no filling at 100 mm Hg (OPP = 0), and totally recovered when the IOP was returned to baseline.

Effect of elevated IOP on total retinal blood flow

Assessment of total RBF in 7 of these animals was achieved through Doppler OCT analysis (Fig. 6). Qualitatively, the signal for arteries (mostly red) and veins (mostly green) appeared to decrease gradually as IOP increased from 10 to 100 mm Hg (Fig. 6A), as compared to companion microangiograms of NFL/GCL and OPL (Fig. 6B top and bottom, respectively). We found that the major arterial branches exhibited labored pulsation with the cardiac cycle as indicated by the white arrows in Fig. 6A. This process was particularly obvious above 70 mm Hg, as the blood flow direction changed between red and green with the cardiac cycle.

The relative change of total RBF in response to sequential IOP elevation is shown in Fig. 7. Total RBF was not affected at the lower levels of IOP elevation (<30 mm Hg). (Fig. 7A) However, above 30 mm Hg, total RBF decreased almost linearly with the increase of IOP, reaching 50% of baseline at 60 mm Hg. Fig. 7B shows the relationship between total RBF and OPP when IOP was increased in 10 mm Hg increments. Total RBF did not change as long as the perfusion pressure was above 80 mm Hg. Below 80 mm Hg, total RBF decreased linearly to zero, reaching 50% of baseline at OPP 40 mm Hg ($R^2 = 0.96$).

Effect of reduced MAP on retinal capillary filling and total RBF

The level of MAP can also influence retinal and ONH blood flow. In order to determine if OMAG/OCT can detect similar relationships in retinal capillary filling and total RBF, we performed measurements in 7 additional animals. In these, we used an identical isoflurane anesthesia, with the exception that the removal of expired gas was passive, leading to an F/air canister (A.M. Bickford, Inc. Wales Center, NY), without active suction. This resulted in a lower MAP, ranging from 65–80 mm Hg (mean = 75 ± 6 mm Hg), presumably due to systemic buildup of CO_2 (Srinivasan et al., 2010). At this lower pressure, the effect of increasing IOP from 10 mm Hg to 100 mm Hg, and then back to 10 mm Hg, on retinal capillary filling was also measured.

Fig. 8 shows quantification of OPL capillary density and total RBF vs IOP and OPP in these animals. Compared to Fig. 5A, an IOP of only 40 mm Hg, as opposed to 60 mm Hg, was sufficient to reduce capillary density below 80% of baseline and 50 mm Hg, rather than 70, reduced it to 60% of baseline (Fig. 8A). IOP appeared to have a greater effect on capillary density than in animals with higher pressure, by an amount nearly equal to the difference in MAP (25 mm Hg) between these two groups. Fig. 8B illustrates density vs OPP. Here, the relationship between density and perfusion pressure was essentially the same as that shown for Fig. 5B, with capillary filling not falling below 60% until perfusion pressure dropped below 30 mm Hg.

The effect of IOP on total RBF was also determined in animals with reduced MAP. Fig. 8C indicates that, similar to animals with higher MAP (Fig. 7A), total RBF decreased linearly, except that this decrease was noted to begin at just above IOP 10 mm Hg, as opposed to 30 mm Hg, with an IOP of 40 mm Hg, rather than 60 mm Hg, reducing TBF to 50% of baseline. Total RBF vs perfusion pressure also decreased linearly (Fig. 8D). There was also a linear relationship between total RBF and OPP similar to that observed in animals with a higher MAP (Fig. 7B), with total RBF reduced to 50% of baseline levels at an OPP of 40 mm Hg.

Increased IOP therefore has a greater impact upon retinal capillary filling in animals with lower MAP, consistent with the observations of He et al. (2012). This suggests that OPP is the principal determinant of blood flow change rather than IOP itself. Maintaining a normal systemic blood pressure is therefore important when studying the effect of IOP on blood flow within the retina as well as the optic nerve head.

Discussion

In our previous work (Zhi et al., 2012a; An et al., 2010), we utilized a SLD light source centered at 1300 nm in order to increase the penetration of light into the ONH. However, this impairs resolution and limits the capability of the system to resolve detailed retinal capillary networks. In order to improve resolution, we elected to use the central wavelength of light source at 1300 nm, which improved the axial resolution to ~7 μm. In addition, the lateral resolution was also improved to ~10 μm. Another modification was to improve the field of view (3×3 mm^2) by using an ocular lens in the sample arm. The improved performance and resolution enabled better visualization of the retinal capillary beds within

three different retinal layers (NFL/GLC, IPL and OPL), and allowed us to quantitatively assess the response of capillaries to elevated IOP.

All measurements were compared against systemic blood pressure. Liang et al. (2009a) showed that elevated IOP reduced blood flow in the optic nerve head of non-human primates only when systemic blood pressure was reduced. He et al. (2012) also demonstrated this effect at a functional level. They showed that retinal ganglion cell function, as determined by the scotopic threshold response (STR) of the electroretinogram, was less susceptible to an IOP challenge with high MAP compared to low MAP. In the current work, monitoring MAP during the entire process of IOP elevation provided us with an opportunity to investigate how different levels of systemic blood pressure would affect the response of retinal capillary density and total retinal blood flow to an IOP elevation challenge. The relationship of both parameters to IOP was affected by an amount equal to the difference in systemic blood pressure, so that their relationship to OPP was unchanged. This is also in agreement with the findings of He et al., using laser Doppler flowmetry, which, in the rat, more generally documents flow in the choroid as well as the retina (He et al., 2012).

There is a complex interplay between OPP and ocular blood flow (He et al., 2012). Autoregulation of blood flow within the lower range of IOP elevation (less than 30 mm Hg) is likely to be responsible for the observed stability of total RBF as well as retinal capillary density in this range. Larger retinal vessels do not receive neural innervation and therefore require local vascular changes to maintain constant blood flow in the context of varying OPP. The caliber of retinal arterioles changes with alterations in OPP with an increase leading to vasoconstriction (Jeppesen et al., 2007) and reduction leading to vasodilatation (Nagel and Vilser, 2004). Studies in human subjects suggest that these autoregulatory mechanisms controlling RBF break down at a threshold IOP above 30 mm Hg (Riva et al., 1986; Schulte et al., 1996) which parallels our observations of total RBF in this study.

Our data also show that capillary filling in the OPL (and, qualitatively, the NFL/GCL and IPL as well) is more resistant than total RBF to a reduced OPP. We found a linear reduction in total RBF when the OPP fell below 80 mm Hg, whereas capillary density in the OPL was maintained above 80% of normal as long as OPP was above 40 mm Hg. This is consistent with our previous report, using a 1300 nm system, where we noted that ONH perfusion did not begin to substantially decrease until IOP exceeded 60 mm Hg (Zhi et al., 2012a), while retinal blood flow decreased linearly once IOP exceeded 30 mm Hg. However, in that study we did not have the ability to assess retinal capillary filling.

He and colleagues (He et al., 2012) noted a similar relationship between OPP and different components of the ERG, in which neither the b-wave nor the STR showed substantial reductions until OPP was below 60 and 40 mm Hg, respectively, in animals with MAP comparable to those studied here. Later, it was found that IOP elevations of 90 min did not produce permanent changes in any ERG parameter until IOP exceeded 60 mm Hg, corresponding to an OPP of 40 mm Hg (Bui et al., 2013). In order to explain the apparent divergence between retinal function and blood flow, this group subsequently proposed a model whereby preserved function with the increase of IOP is accomplished by the increase

of oxygen extraction (He et al., 2013). The ability to visualize individual retinal capillary beds in the current study provides anatomic support for this hypothesis, since the persistent density of capillaries observed here in the face of reduced total retinal blood flow would suggest that red blood cell transit will be slowed, which would allow greater oxygen extraction.

At present, our system does not provide the ability to detect such subtle changes in capillary flow. OMAG has ultra-high sensitivity to blood flow, allowing the detection of slow flow down to 4 μm/s (Brownian motion level) (An et al., 2010). As long as there is flow, even in capillaries, it will be imaged by OMAG. Only when RBCs stop flowing will capillaries disappear in the flow image. Thus, it is possible that decreases in capillary flow speed/flux, which would allow increased oxygen extraction, may occur but not be evident from the angiography image. A method of quantifying RBC flow speed and flux within retinal capillaries would be necessary to resolve this issue. OCT has been utilized to measure the RBC velocity and flux of capillaries within cerebrovascular networks in mouse brains (Lee et al., 2013) and future work will develop similar techniques utilizing OCT to measure the capillary RBC flow speed/flux within the rodent retina and determine the effect of increased IOP (and reduced OPP) on this important parameter.

The results of this study have a direct bearing on glaucoma, since ischemia has long been suspected to contribute to optic nerve damage in this disease (Alm and Bill, 1972; Pillunat et al., 1996, 1997; Liang et al., 2009a). Recent work has shown that OCT angiography of the optic disk (Chen et al., 2015; Jia et al., 2014) and peripapillary retinal nerve fiber layer may provide sensitive clinical measures of glaucoma severity. Our current findings show that, in rats, retinal capillary filling, similar to previous studies in the ONH (Zhi et al., 2012a) is preserved at IOPs as high as 60 mm Hg in animals with normal blood pressure. This strongly suggests that current efforts to model this disease using acute IOP elevations to this range for several hours (Abbott et al., 2014; Morrison et al., 2014) are unlikely to produce optic nerve damage via purely ischemic mechanisms.

Conclusion

The effect of elevated IOP on the retinal capillary bed filling and total RBF has been evaluated by OMAG/OCT. OMAG allows the imaging of the retinal capillary microvasculature within different retinal layers, permitting noninvasive monitoring of the response to elevated IOP, and Doppler OCT is able to measure the total retinal blood flow. We demonstrated that reduced systemic blood pressure can modify the retinal blood flow susceptibility to IOP elevation by reducing OPP. The results show that both total RBF and capillary beds were not affected at the lower levels of IOP elevation (<30 mm Hg) and higher levels of OPP (>60 mm Hg), which may represent vascular autoregulation of ocular blood flow. However, differing sensitivity to a reduction in OPP was seen between the retinal capillaries and total blood flow within the large caliber vessels suggesting the involvement of discrete autoregulatory mechanisms so that capillary patency and flow is maintained over a wide range of OPP.

Acknowledgments

This work was supported by the NIH/NEI grants R01EY024158 (RKW), R01EY010145 (JCM), P30EY010572 (JCM), and Unrestricted Grants from Research to Prevent Blindness (RPB), including an Innovative RPB Research Award to RKW. HJ is supported by an award by the Fulbright Commission in conjunction with Fight for Sight.

References

Abbott CJ, Choe TE, Lusardi TA, Burgoyne CF, Wang L, Fortune B. Evaluation of retinal nerve fiber layer thickness and axonal transport 1 and 2 weeks after 8 hours of acute intraocular pressure elevation in rats. Invest. Ophthalmol. Vis. Sci. 2014; 55:674–687. [PubMed: 24398096]

Alm A, Bill A. The oxygen supply to the retina. II. Effects of high intraocular pressure and of increased arterial carbon dioxide tension on uveal and retinal blood flow in cats. A study with radioactively labelled microspheres including flow determinations in brain and some other tissues. Acta Physiol. Scand. 1972; 84:306–319. [PubMed: 4553229]

An L, Qin J, Wang RK. Ultrahigh sensitive optical microangiography for in vivo imaging of microcirculations within human skin tissue beds. Opt. Express. 2010; 18:8220–8228. [PubMed: 20588668]

Balaratnasingam C, Morgan WH, Bass L, Matich G, Cringle SJ, Yu DY. Axonal transport and cytoskeletal changes in the laminar regions after elevated intraocular pressure. Invest. Ophthalmol. Vis. Sci. 2007; 48:3632–3644. [PubMed: 17652733]

Balaratnasingam C, Morgan WH, Bass L, McKnight C, Cringle SJ, Yu DY. Elevated pressure induced astrocyte damage in the optic nerve. Brain Res. 2008; 1244:142–154. [PubMed: 18848926]

Bui BV, Edmunds B, Cioffi GA, Fortune B. The gradient of retinal functional changes during acute intraocular pressure elevation. Invest. Ophthalmol. Vis. Sci. 2005; 46:202–213. [PubMed: 15623775]

Bui BV, Batcha AH, Fletcher E, Wong VH, Fortune B. Relationship between the magnitude of intraocular pressure during an episode of acute elevation and retinal damage four weeks later in rats. PLoS One. 2013; 8:e70513. [PubMed: 23922999]

Chen CL, Gupta D, Wen JC, et al. Optic disc perfusion in glaucoma with optical microangiography (OMAG). Invest. Ophthalmol. Vis. Sci. 2015; 56(7):1310–1310. [PubMed: 25587062]

Cuthbertson RA, Mandel TE. Anatomy of the mouse retina — endothelial-cell pericyte ratio and capillary distribution. Invest. Ophthalmol. Vis. Sci. 1986; 27:1659–1664. [PubMed: 3771146]

Ffytche T, Bulpitt C, Kohner E, Archer D, Dollery C. Effect of changes in intraocular pressure on the retinal microcirculation. Br. Med. J. 1974; 58:514.

Fortune B, Bui BV, Morrison JC, Jobnson EC, Dong F, Cepurna WO, Jia LJ, Barber S, Cioffi GA. Selective ganglion cell functional loss in rats with experimental glaucoma. Invest. Ophthalmol. Vis. Sci. 2004; 45:1854–1862. [PubMed: 15161850]

Fortune B, Choe TE, Reynaud J, Hardin C, Cull GA, Burgoyne CF, Wang L. Deformation of the rodent optic nerve head and peripapillary structures during acute intraocular pressure elevation. Invest. Ophthalmol. Vis. Sci. 2011; 52:6651–6661. [PubMed: 21730343]

Guedes V, Schuman JS, Hertzmark E, Wollstein G, Correnti A, Mancini R, Lederer D, Voskanian S, Velazquez L, Pakter HM, Pedut-Kloizman T, Fujimoto JG, Mattox C. Optical coherence tomography measurement of macular and nerve fiber layer thickness in normal and glaucomatous human eyes. Ophthalmology. 2003; 110:177–189. [PubMed: 12511364]

Guo L, Normando EM, Nizari S, Lara D, Cordeiro MF. Tracking longitudinal retinal changes in experimental ocular hypertension using the cSLO and spectral domain-OCT. Invest. Ophthalmol. Vis. Sci. 2010; 51:6504–6513. [PubMed: 20688741]

He Z, Vingrys AJ, Armitage JA, Bui BV. The role of blood pressure in glaucoma. Clin. Exp. Optom. 2011; 94:133–149. [PubMed: 21255075]

He Z, Nguyen CTO, Armitage JA, Vingrys AJ, Bu BV. Blood pressure modifies retinal susceptibility to intraocular pressure elevation. PLoS One. 2012; 7(2):e31104. http://dx.doi.org/10.1371/journal.pone.0031104. [PubMed: 22359566]

He Z, Lim JK, Nguyen CT, Vingrys AJ, Bui BV. Coupling blood flow and neural function in the retina: a model for homeostatic responses to ocular perfusion pressure challenge. Physiol. Rep. 2013; 1:e00055. [PubMed: 24303137]

Huang D, Swanson EA, Lin CP, Schuman JS, Stinson WG, Chang W, Hee MR, Flotte T, Gregory K, Puliafito CA, et al. Optical coherence tomography. Science. 1991; 254:1178–1181. [PubMed: 1957169]

Jeppesen P, Knudsen ST, Poulsen PL, Mogensen CE, Schmitz O, Bek T. Response of retinal arteriole diameter to increased blood pressure during acute hyperglycaemia. Acta Ophthalmol. Scand. 2007; 85:280–286. [PubMed: 17488457]

Jia Y, Wei E, Wang X, et al. Optical coherence tomography angiography of optic disc perfusion in glaucoma. Ophthalmology. 2014; 121:1322–1332. [PubMed: 24629312]

Johnson EC, Doser TA, Cepurna WO, Dyck JA, Jia L, Guo Y, Lambert WS, Morrison JC. Cell proliferation and interleukin-6 type cytokine signaling characterize gene expression responses in early optic nerve head injury in rat glaucoma. Invest. Ophthalmol. Vis. Sci. 2011; 52:504–518. [PubMed: 20847120]

Kanamori A, Nakamura M, Escano MFT, Seya R, Maeda H, Negi A. Evaluation of the glaucomatous damage on retinal nerve fiber layer thickness measured by optical coherence tomography. Am J. Ophthalmol. 2003; 135:513–520. [PubMed: 12654369]

Kim IB, Kim KY, Joo CK, Lee MY, Oh SJ, Chung JW, Chun MH. Reaction of Muller cells after increased intraocular pressure in the vet retina. Exp. Brain Res. 1998; 121:419–424. [PubMed: 9746148]

Kong YX, van Bergen N, Trounce IA, Bui BV, Chrysostomou V, Waugh H, Vingrys A, Crowston JG. Increase in mitochondrial DNA mutations impairs retinal function and renders the retina vulnerable to injury. Aging Cell. 2011; 10:572–583. [PubMed: 21332926]

Kong YX, van Bergen N, Bui BV, Chrysostomou Y, Vingrys AJ, Trounce IA, Crowston JG. Impact of aging and diet restriction on retinal function during and after acute intraocular pressure injury. Neurobiol. Aging. 2012; 33(6):e15–e25. http://dx.doi.org/10.1016/j.neurobiolaging.2011.11.026 (1126). [PubMed: 22217415]

Lee J, Wu WC, Lesage F, Boas DA. Multiple-capillary measurement of RBC speed, flux, and density with optical coherence tomography. J. Cereb. Blood Flow Metab. 2013; 33:1707–1710. [PubMed: 24022621]

Liang Y, Downs JC, Fortune B, Cull G, Cioffi GA, Wang L. Impact of systemic blood pressure on the relationship between intraocular pressure and blood flow in the optic nerve head of nonhuman primates. Invest. Ophthalmol. Vis. Sci. 2009a; 50:2154–2160. [PubMed: 19074806]

Liang Y, Downs JC, Fortune B, Cull G, Cioffi GA, Wang L. Impact of systemic blood pressure on the relationship between intraocular pressure and blood flow in the optic nerve head of nonhuman primates. Invest. Ophthalmol. Vis. Sci. 2009b; 50:2154–2160. [PubMed: 19074806]

Morrison JC, Moore CG, Deppmeier LMH, Gold BG, Meshul CK, Johnson EC. A rat model of chronic pressure-induced optic nerve damage. Exp. Eye Res. 1997; 64:85–96. [PubMed: 9093024]

Morrison JC, Johnson EC, Cepurna W, Jia LJ. Understanding mechanisms of pressure-induced optic nerve damage. Prog. Retin. Eye Res. 2005; 24:217–240. [PubMed: 15610974]

Morrison JC, Johnson E, Cepurna WO. Rat models for glaucoma research. Prog. Brain Res. 2008; 173:285–301. [PubMed: 18929117]

Morrison JC, Cepurna WO, Guo Y, Johnson EC. Pathophysiology of human glaucomatous optic nerve damage: insights from rodent models of glaucoma. Exp. Eye Res. 2011; 93(2):154–164.

Morrison JC, Choe TE, Cepurna WO, Johnson EC. Optic nerve head gene expression responses to elevated intraocular pressure, anesthesia and anterior chamber cannulation in the controlled elevation of IOP model-induced optic nerve injury. Invest. Ophthalmol. Vis. Sci. 2014; 54:2402. (E-Abstract).

Nagel E, Vilser W. Autoregulative behavior of retinal arteries and veins during changes of perfusion pressure: a clinical study. Graefes Arch. Clin. Exp. Ophthalmol. 2004; 242:13–17. [PubMed: 14648137]

Pang IH, Clark AF. Rodent models for glaucoma retinopathy and optic neuropathy. J. Glaucoma. 2007; 16:483–505. [PubMed: 17700292]

Pillunat LE, Anderson DR, Knighton RW, Joos KM, Feuer WJ. Dynamic response of optic nerve head blood flow to increased intraocular pressure. Invest. Ophthalmol. Vis. Sci. 1996; 37:2098–2098.

Pillunat LE, Anderson DR, Knighton RW, Joos KM, Feuer WJ. Autoregulation of human optic nerve head circulation in response to increased intraocular pressure. Exp. Eye Res. 1997; 64:737–744. [PubMed: 9245904]

Pinhas A, Razeen M, Dubow M, Gan A, Chui TY, Shah N, Mehta M, Gentile RC, Weitz R, Walsh JB, Sulai YN, Carroll J, Dubra A, Rosen RB. Assessment of perfused foveal microvascular density and identification of nonperfused capillaries in healthy and vasculopathic eyes. Invest. Ophthalmol. Vis. Sci. 2014; 55:8056–8066. [PubMed: 25414179]

Quigley HA, Broman AT. The number of people with glaucoma worldwide in 2010 and 2020. Br. J. Ophthalmol. 2006; 90:262–267. [PubMed: 16488940]

Reif R, Qin J, An L, Zhi Z, Dziennis S, Wang R. Quantifying optical microangiography images obtained from a spectral domain optical coherence tomography system. J. Biomed. Imaging. 2012; 509783 2012. http://dx.doi.org/10.1155/2012/509783.

Riva CE, Grunwald JE, Petrig BL. Autoregulation of human retinal blood flow. An investigation with laser Doppler velocimetry. Invest. Ophthalmol. Vis. Sci. 1986; 27:1706–1712. [PubMed: 2947873]

Roberts MD, Sigal IA, Liang Y, Burgoyne CF, Downs JC. Changes in the biomechanical response of the optic nerve head in early experimental glaucoma. Invest. Ophthalmol. Vis. Sci. 2010; 51:5675–5684. [PubMed: 20538991]

Roorda A, Romero-Borja F, Donnelly WJ, Queener H, Hebert TJ, Campbell MCW. Adaptive optics scanning laser ophthalmoscopy. Opt. Express. 2002; 10:405–412. [PubMed: 19436374]

Ruggeri M, Webbe H, Jiao SL, Gregori G, Jockovich ME, Hackam A, Duan YL, Puliafito CA. In vivo three-dimensional high-resolution imaging of rodent retina with spectral-domain optical coherence tomography. Invest. Ophthalmol. Vis. Sci. 2007; 48:1808–1814. [PubMed: 17389515]

Ruusuvaa P, Palkama A. Effect of short-term increased intraocular-pressure on fine-structure of retina. Acta Ophthalmol. Suppl. 1974; 123:41–46. [PubMed: 4368633]

Schulte K, Wolf S, Arend O, Harris A, Henle C, Reim M. Retinal hemodynamics during increased intraocular pressure. Ger. J. Ophthalmol. 1996; 5:1–5. [PubMed: 8646172]

Schuman JS, Hee MR, Puliafito CA, Wong C, Pedutkloizman T, Lin CP, Hertzmark E, Izatt JA, Swanson EA, Fujimoto JG. Quantification of nerve-fiber layer thickness in normal and glaucomatous eyes using optical coherence tomography — a pilot-study. Arch. Ophthalmol.-Chic. 1995; 113:586–596.

Shepherd AP, Riedel GL. Continuous measurement of intestinal mucosal blood flow by laser-Doppler velocimetry. Am. J. Physiol. 1982; 242:G668–G672. [PubMed: 7091339]

Sommer A. Intraocular-pressure and glaucoma. Am J. Ophthalmol. 1989; 107:186–188. [PubMed: 2913813]

Srinivasan VJ, Ko TH, Wojtkowski M, Carvalho M, Clermont A, Bursell SE, Song QH, Lem J, Duker JS, Schuman JS, Fujimoto JG. Noninvasive volumetric Imaging and morphometry of the rodent retina with high-speed, ultrahigh-resolution optical coherence tomography. Invest. Ophthalmol. Vis. Sci. 2006; 47:5522–5528. [PubMed: 17122144]

Srinivasan VJ, Sakadzic S, Gorczynska I, Ruvinskaya S, Wu W, Fujimoto JG, Boas DA. Quantitative cerebral blood flow with optical coherence tomography. Opt. Express. 2010; 18:2477–2494. [PubMed: 20174075]

Strouthidis NG, Fortune B, Yang HL, Sigal IA, Burgoyne CF. Longitudinal change detected by spectral domain optical coherence tomography in the optic nerve head and peripapillary retina in experimental glaucoma. Invest. Ophthalmol. Vis. Sci. 2011; 52:1206–1219. [PubMed: 21217108]

Sun D, Qu J, Jakobs TC. Reversible reactivity by optic nerve astrocytes. Glia. 2013; 61:1218–1235. [PubMed: 23650091]

Tomolins PH, Wang RK. Theory, developments and applications of optical coherence tomography. J. Phys. D. Appl. Phys. 2005; 38(15):2519–2535.

Vidal L, Diaz F, Villena A, Moreno M, Campos JG, de Vargas IP. Nitric oxide synthase in retina and optic nerve head of rat with increased intraocular pressure and effect of timolol. Brain Res. Bull. 2006; 70:406–413. [PubMed: 17027776]

Wang RK, Jacques SL, Ma Z, Hurst S, Hanson SR, Gruber A. Three dimensional optical angiography. Opt. Express. 2007; 15:4083–4097. [PubMed: 19532651]

Wang RK, An L, Francis P, Wilson DJ. Depth-resolved imaging of capillary networks in retina and choroid using ultrahigh sensitive optical microangiography. Opt. Lett. 2010; 35:1467–1469. [PubMed: 20436605]

Yancey CM, Linsenmeier RA. Oxygen distribution and consumption in the cat retina at increased intraocular-pressure. Invest. Ophthalmol. Vis. Sci. 1989; 30:600–611. [PubMed: 2703301]

Yin X, Chao JR, Wang RKK. User-guided segmentation for volumetric retinal optical coherence tomography images. J. Biomed. Opt. 2014; 19(8):086020. http://dx.doi.org/10.1117/1.JBO.19.8.086020. [PubMed: 25147962]

Yousefi S, Zhi Z, Wang RK. Eigendecomposition-based clutter filtering technique for optical microangiography. IEEE Trans. Biomed. Eng. 2011; 58:2316–2323.

Zeimer RC. The relation between glaucomatous damage and optic-nerve head mechanical compliance. Arch. Ophthalmol.-Chic. 1989; 107:1232–1234.

Zhi Z, Cepurna W, Johnson E, Shen T, Morrison J, Wang RK. Volumetric and quantitative imaging of retinal blood flow in rats with optical microangiography. Biomed. Opt. Express. 2011; 2:579–591. [PubMed: 21412463]

Zhi Z, Cepurna WO, Johnson EC, Morrison JC, Wang RK. Impact of intraocular pressure on changes of blood flow in the retina, choroid, and optic nerve head in rats investigated by optical microangiography. Biomed. Opt. Express. 2012a; 3:2220–2233. [PubMed: 23024915]

Zhi Z, Yin X, Dziennis S, Wietecha T, Hudkins KL, Alpers CE, Wang RK. Optical microangiography of retina and choroid and measurement of total retinal blood flow in mice. Biomed. Opt. Express. 2012b; 3:2976–2986. [PubMed: 23162733]

Zhi Z, Chao J, Wietecha T, Hudkins K, Alpers C, Wang R. Noninvasive imaging of retinal morphology and microvasculature in obese mice using optical coherence tomography and optical microangiography. Invest. Ophthalmol. Vis. Sci. 2014; 55(2):1024–1030. [PubMed: 24458155]

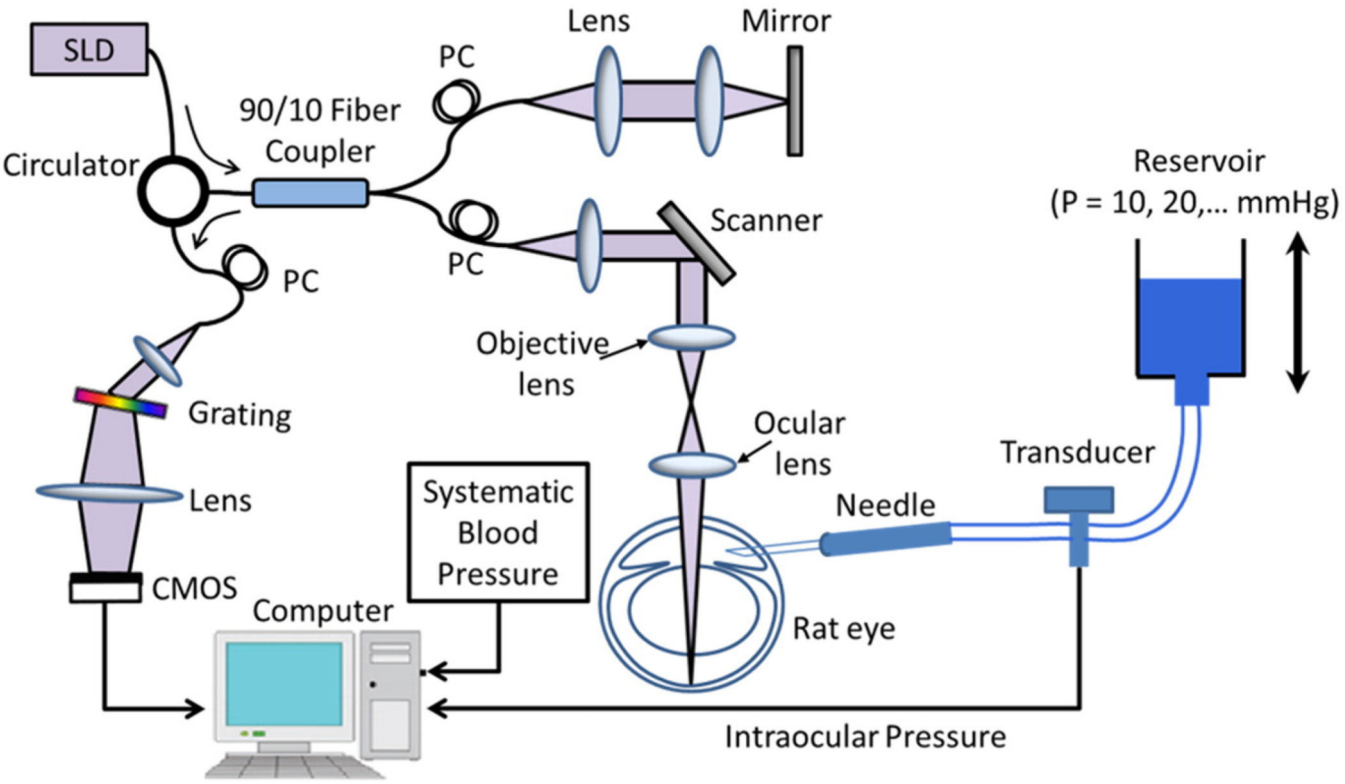

Fig. 1.

Schematic of the setup utilizing a high-speed spectral domain OCT system for in vivo imaging of a rat eye under controlled intraocular pressure. SLD: superluminescent diode; PC: polarization controller; CMOS: line scan camera.

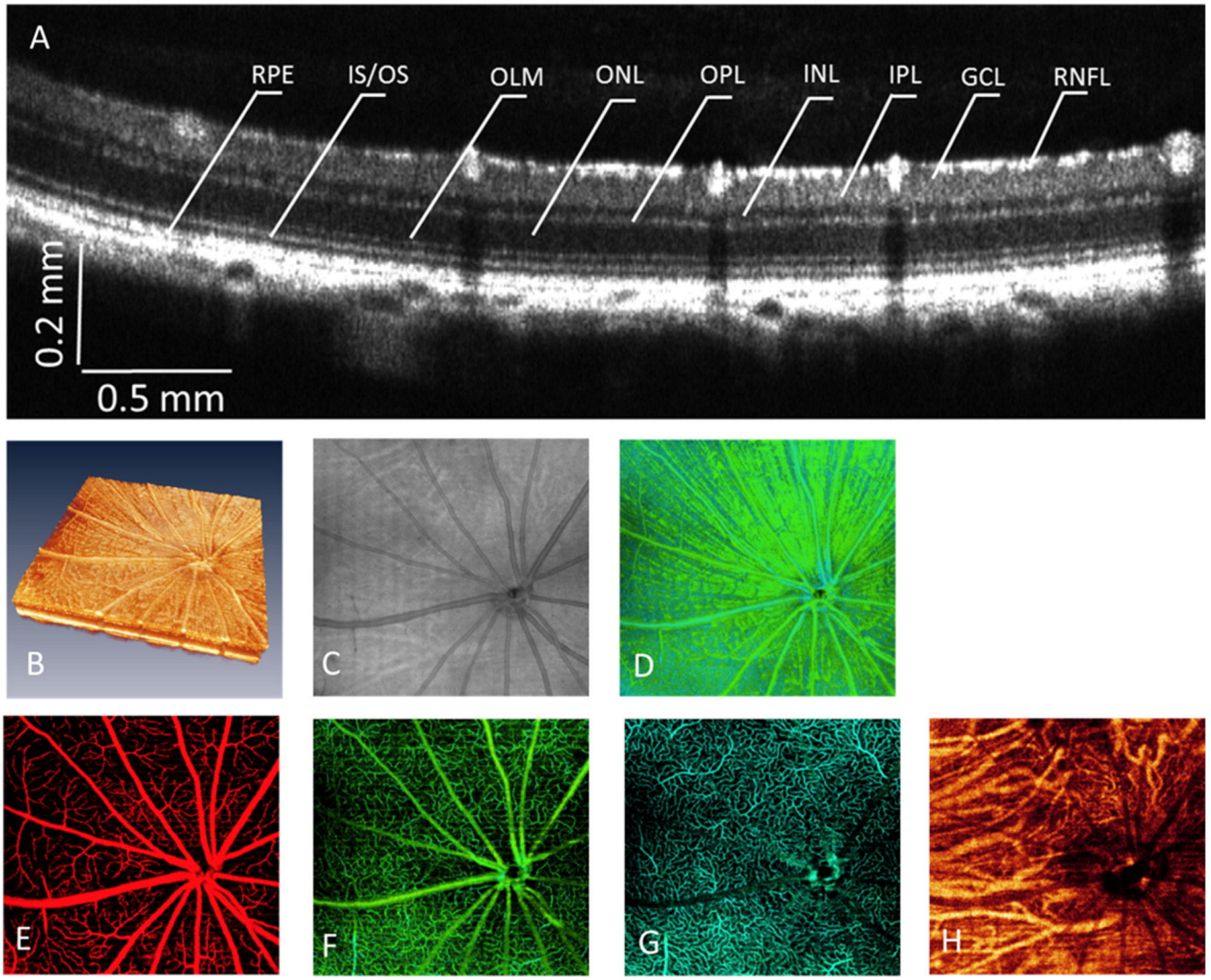

Fig. 2.

Details of the rat retina visualized by OMAG/OCT. (A) Cross-sectional OCT structure image, illustrating all the retinal layers, NFL: nerve fiber layer, GCL: ganglion cell layer, IPL: inner plexiform layer, INL: inner nuclear layer, OPL: outer plexiform layer, ONL: outer nuclear layer, OLM: outer limiting membrane, IS/OS: inner/outer segment, RPE: retinal pigment epithelium. (B) 3D volume rendering of the retina structure. (C) OCT fundus image. (D) Projection view of NFL, showing the nerve fiber bundles. (E–H) Depth-resolved detailed microangiogram with OMAG, showing microvasculature/capillaries within NFL/GCL (E), capillary network within IPL (F), capillary network within OPL (G), and vasculature within choroid (H).

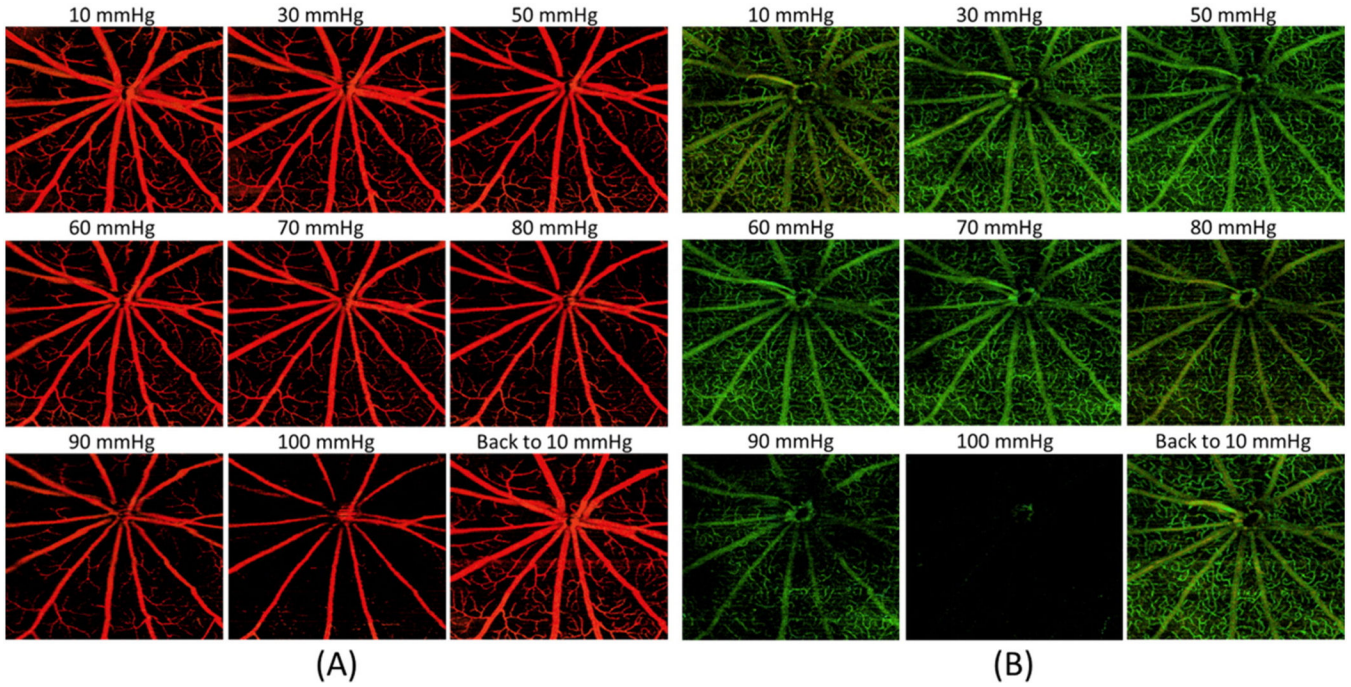

Fig. 3.

Response of micro-vessels/capillaries to elevated IOP within the (A) NFL/GCL and (B) IPL. In both, vascular filling does not show qualitative changes until IOP exceeds 60–70 mm Hg.

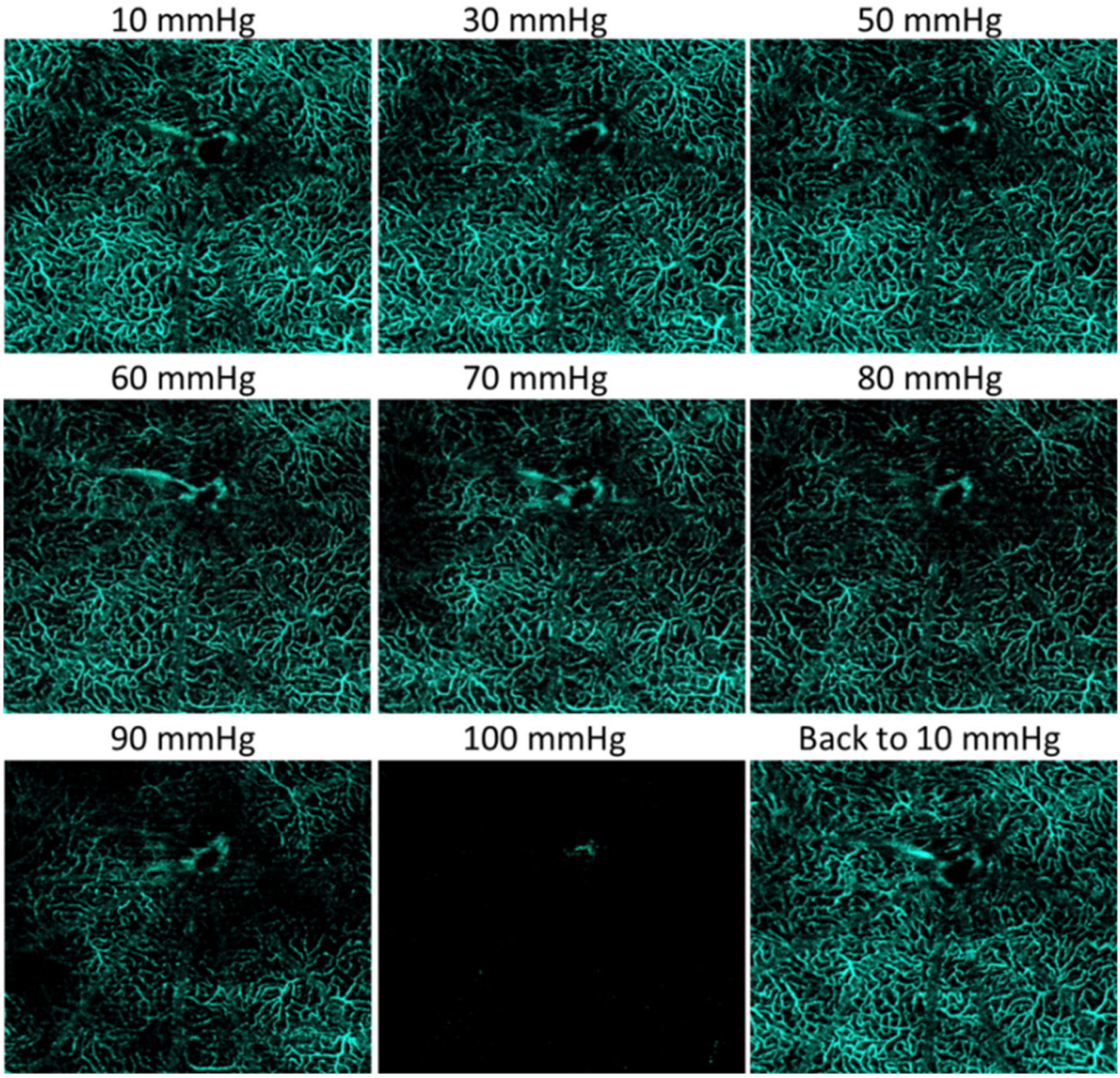

Fig. 4.

The response of capillaries within OPL to elevated IOP. The capillary density appears relatively stable until IOP exceeds 60–70 mm Hg.

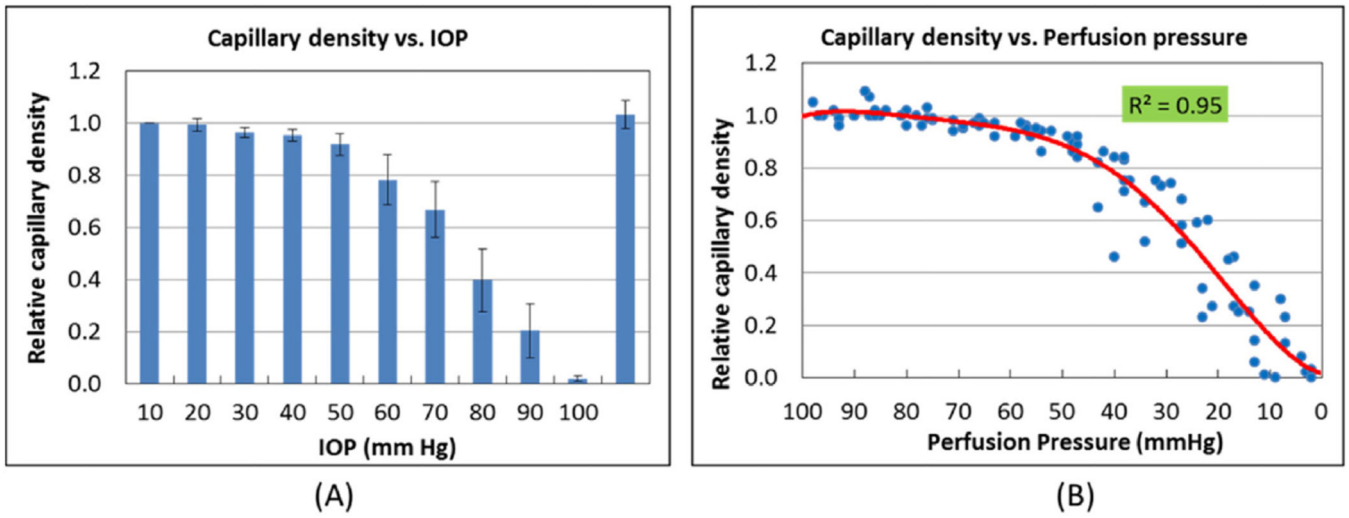

Fig. 5.

(A) OPL capillary density vs IOP shows that density is relatively preserved up to 60 mm Hg but begins to decrease sharply above this level, reaching approximately 60% of normal at 70 mm Hg. Data are shown as mean ± SD (N = 10). Reducing IOP to baseline (10 mm Hg) fully restores capillary density. (B) Capillary density plotted against OPP indicates that capillary density does not decrease below 60% until ocular perfusion pressure is less than 30 mm Hg.

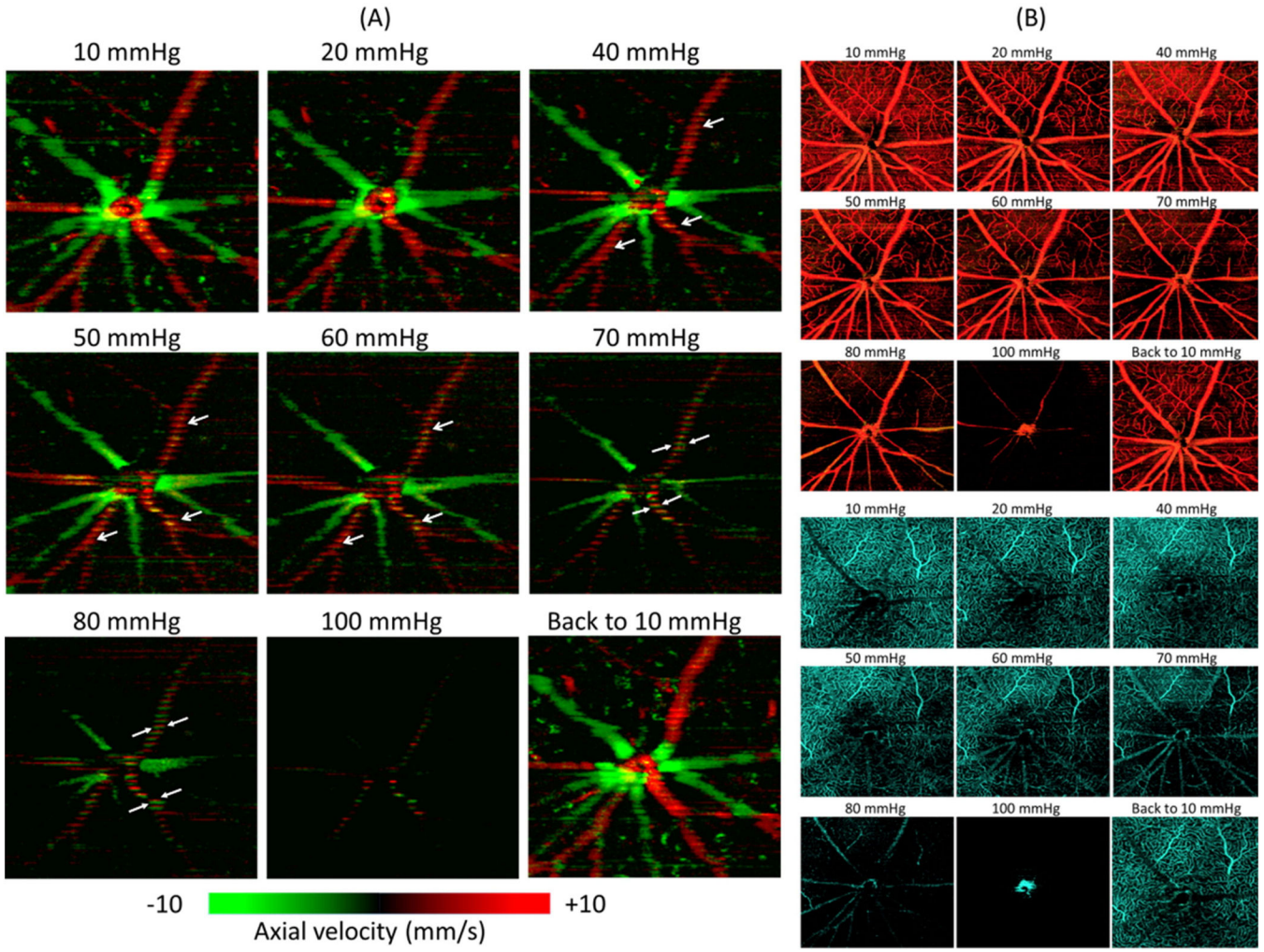

Fig. 6.

(A) Phase-resolved Doppler flow images for total RBF measurement under stepwise increased IOP. Red means flow towards the reader (artery) and green means flow away from the reader (vein). White arrows show the pulsatile flow in the retinal arterioles. (B) Microangiograms of NFL/GCL (top) and OPL (bottom) capillary pattern responses to IOP elevation (for comparison with total RBF). (For interpretation of the references to color in this figure legend, the reader is referred to the web version of this article.)

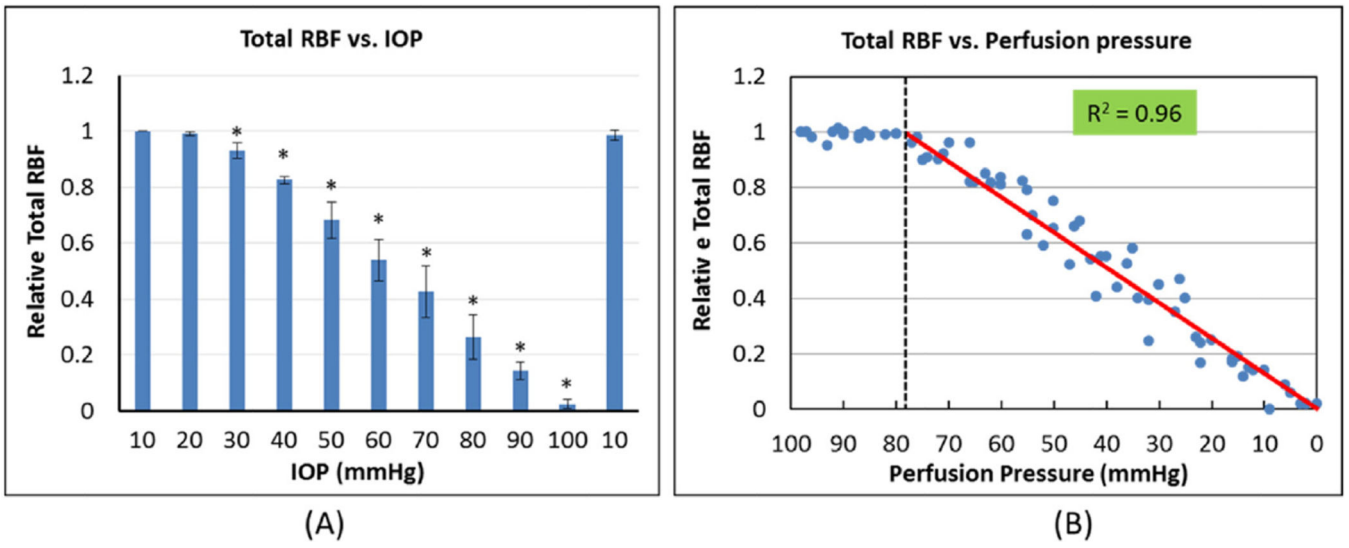

Fig. 7.

(A) Total RBF decreases with the increase of IOP, beginning at 30 mm Hg (* indicates significant change compared to prior IOP level). Data are shown as mean ± SD (N = 7). (B) Change in total RBF with the decrease of ocular perfusion pressure shows a linear decrease once perfusion pressure falls below 80 mm Hg (left of the dashed vertical line). Red line indicates linear fit of individual data points.

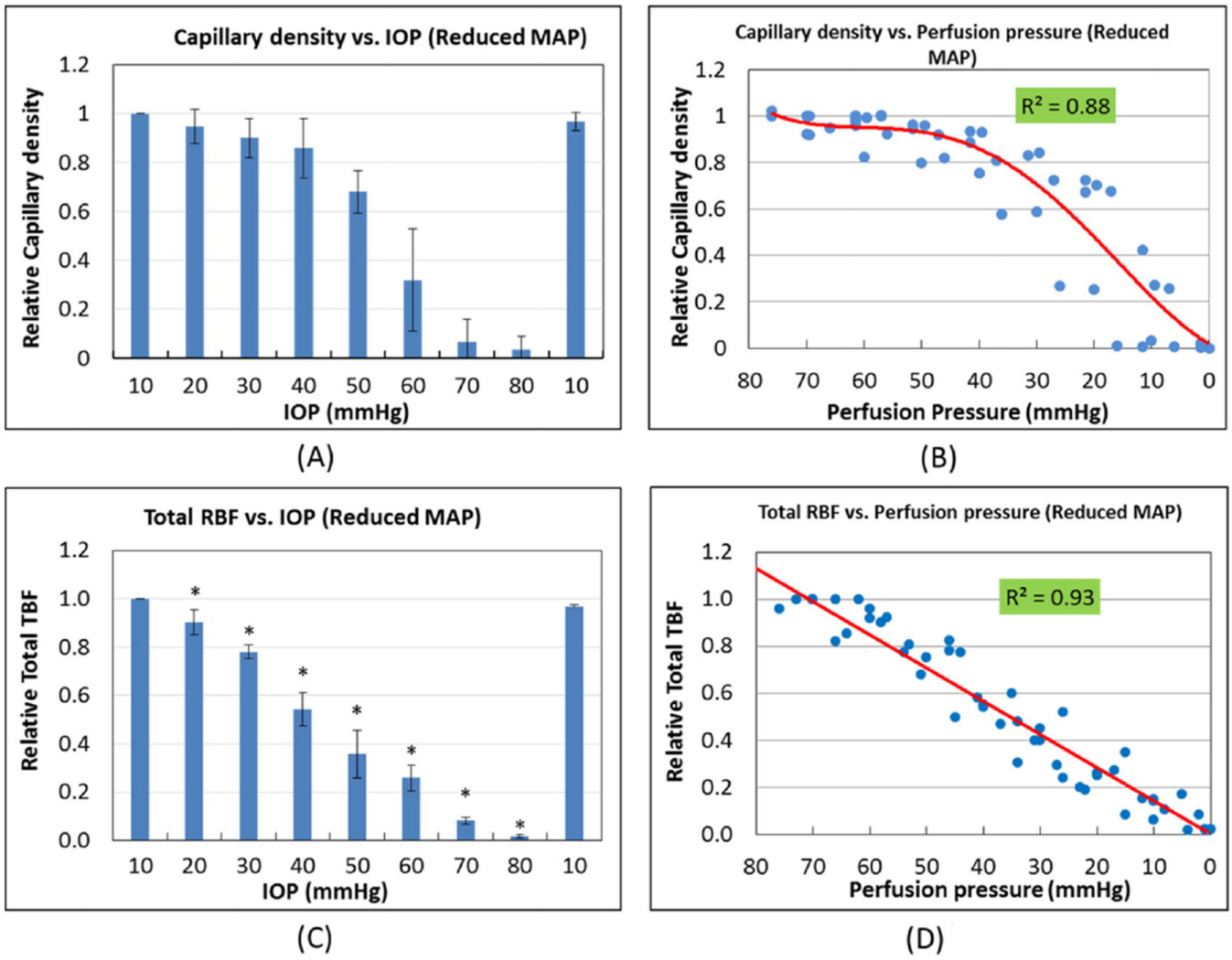

Fig. 8.

Relationship of OPL capillary density and total RBF to IOP (A and C, respectively) and to OPP (B and D, respectively) in animals with reduced MAP. Both parameters show greater sensitivity to a given level of IOP (A and C) as opposed to animals with higher blood pressure, by an amount approximately equal to the difference in MAP between these two groups (20 mm Hg). For both parameters, their relationships to OPP appear unchanged by reduced MAP. (B) Capillary density is preserved at or above 80% of baseline until perfusion pressure falls below 40 mm Hg, followed by a rapid decrease to zero. (D) Total RBF begins a linear decrease once OPP falls below 80 mm Hg, reaching 50% of normal at approximately 40 mm Hg. (N = 7). (C. * indicates significant change compared to prior IOP level).